



# GEOMETRICAL OPTIMIZATION OF A SUPERSONIC LAMINAR NOZZLE FOR ENHANCED AEROTHERMODYNAMICS GROUND TESTING

A. Testa, P. Schrooyen, G. Grossir, and J. Steelant 2

#### Abstract

This paper presents a modular, automated framework for the early-stage aerodynamic optimization of quiet supersonic nozzles, leveraging Bayesian Optimization (BO) to minimize boundary-layer instability growth. The methodology integrates inviscid contour generation via the Method of Characteristics, viscous boundary-layer correction, and local Linear Stability Theory (LST) for transition prediction. The total amplification of first-mode and Görtler instabilities is used as the objective function, with additional constraints on nozzle compactness, manufacturability, and quiet flow length. The BO loop demonstrates rapid convergence within a limited number of evaluations, accurately identifying optimal geometries that satisfy realistic facility constraints. The framework, verified against a previously validated pipeline, reveals key insights into the impact of geometric and thermal parameters—such as throat height, expansion angle, and wall temperature distribution—on transition onset. The approach is flexible and extendable to hypersonic regimes, making it a promising tool for the next-generation guiet tunnel design.

**Keywords:** nozzle, quiet wind tunnel, hypersonics, boundary-layer transition, optimization

#### **Nomenclature**

Latin

B, C – Points identified in Fig. 2

M – Mach number

N - N factor

r – Half height of 2D nozzle geometry, m

 $R_c$  – Throat radius of curvature, m

Re - Reynolds number

T – Temperature, K

x,y - Cartesian coordinates,  $\mathbf{m}$ 

 $x_c$  – Curvilinear coordinate, m

 $X_{BC}$  – Dimensionless distance between B and C 0 – Stagnation conditions

 $x_{\rm BL}$  – Axial location of start of BL computation

Greek

 $\delta^*$  – Boundary-layer displacement thickness, m

 $\omega$  – Maximum nozzle opening angle

 $\Delta x$  – Quiet uniform flow length

Subscripts

1st - 1st mode

Gö – Görtler

 $w \, - \, \operatorname{Wall}$ 

#### 1. Introduction

The development of advanced ground-based facilities for high-speed boundary-layer transition research remains a cornerstone in supersonic and hypersonic aerothermodynamics [1]. These facilities provide critical insight into the physical mechanisms of transition and support the validation of numerical models across a wide range of flow regimes. However, conventional high-speed wind tunnels are limited in their ability to replicate flight-representative conditions due to elevated noise levels, primarily caused by turbulence-induced acoustic radiation from nozzle-wall boundary layers [2, 3]. This discrepancy can significantly impact the natural transition mechanisms and the transition onset location, thereby reducing the fidelity of the ground to flight extrapolation for those experimental data.

To address this issue, the concept of quiet wind tunnels emerged in the 1970s and 1980s through foundational work conducted at NASA. Beckwith and Holley [4] highlighted how concave wall curvature

¹von Karman Institute for Fluid Dynamics, alberto.testa@yki.ac.be - pierre.schrooyen@yki.ac.be quillaume.grossir@vki.ac.be

<sup>&</sup>lt;sup>2</sup>European Space Research and Technology Centre, johan.steelant@esa.int

in supersonic and hypersonic nozzles can trigger Görtler instabilities, stressing the importance of shallow expansions and large curvature radii to minimize Gortler growth rates. Chen, Malik, and Beckwith [5] further investigated the role of both centrifugal and first-mode instabilities using experiments and Linear Stability Theory (LST), establishing a reference amplification threshold of  $N_{\rm crit}\approx7.5$  for transition prediction in low-disturbance environments.

A major step forward was achieved through the work of Schneider, who synthesized previous findings into a comprehensive design methodology for quiet nozzles. His contributions guided the development of the BAM6QT facility and established key design principles—including controlled wall shaping, local throat heating and subsequent wall cooling [6] and contraction-region boundary-layer suction—to maintain laminar wall conditions and suppress radiated disturbances [7]. These strategies have since become standard in quiet nozzle design.

More recently, Lakebrink et al. [8] built upon these concepts by coupling high-fidelity CFD with LST-based instability analysis, embedding the evaluations into a Kriging metamodel loop for design optimization. Their work demonstrated that significant improvements in quiet performance can be achieved through optimization-driven wall shaping. However, the computational demands of full CFD simulations may reduce the practicality of this approach for rapid design iterations or broad parametric explorations.

To provide a more agile alternative in such contexts, the present study builds upon a recently introduced modular and low-cost framework for laminar nozzle design [9], which integrates inviscid contour generation (HYPNOZE [10]), viscous boundary-layer correction (DEKAF [11]) and linear stability analysis (VESTA [12]) into a fast, automatable pipeline. This framework is here embedded within a non-intrusive Bayesian optimization loop, enabling efficient exploration of the design space while minimizing computational cost. The objective is to reduce integrated instability growth (N-factors) and enhance quiet-flow Reynolds numbers and test core uniformity.

The manuscript presents the complete methodology for high-speed nozzle generation and analysis, the design space and optimization objectives and the results of the optimization loop. Final remarks and perspectives for future work are provided in the concluding section.

## 2. Methodology Overview

This section outlines the design and optimization methodology adopted in the present study. The overall pipeline, implemented and verified in [9], is briefly recalled with a focus on the main assumptions and the role of each integrated tool within the framework. In this work, the pipeline has been fully automated to enable seamless coupling with the Bayesian optimization loop, removing the need for user intervention between individual design generation and performance evaluation. For a comprehensive description of the pipeline components and their validation, the reader is referred to [9].

Following this overview, the Bayesian optimization framework is introduced in detail, describing its integration with the high-fidelity simulation tools, surrogate model training and acquisition strategy.

## 2.1. Design pipeline

Figure 1 presents the design pipeline used for high-fidelity evaluations within the optimization loop.

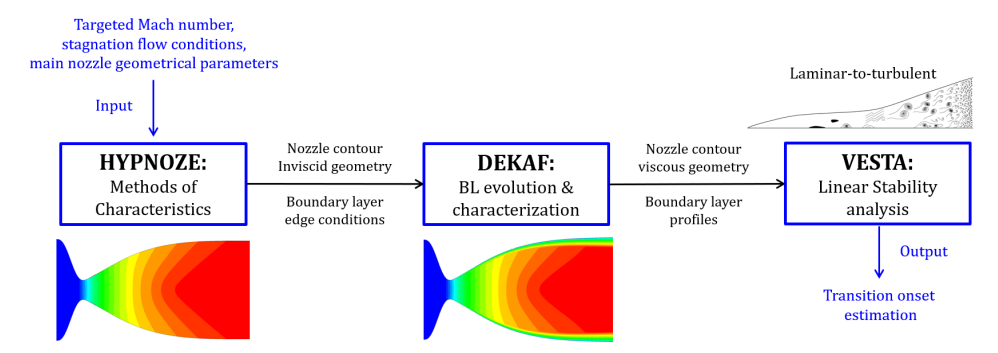


Fig 1. Overview of the computational framework used for nozzle design and optimization.

Given a small set of key geometrical design parameters and boundary conditions (highlighted in red in Figure 2), the first step is performed by the HYPNOZE toolkit that computes the flow expansion and nozzle contoured geometry using a Method of Characteristics based algorithm assuming inviscid flow [10]. The resulting contour and wall flow conditions serve as input to DEKAF, a marching boundary-layer solver that computes laminar profiles along the nozzle wall and computes BL integral lengths, such as  $\delta^*$  used to infer the viscous correction [11].

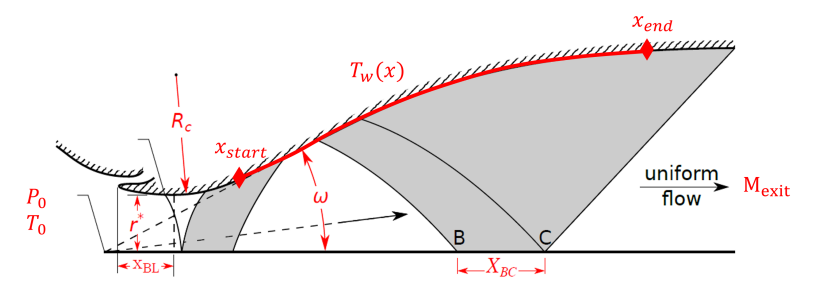
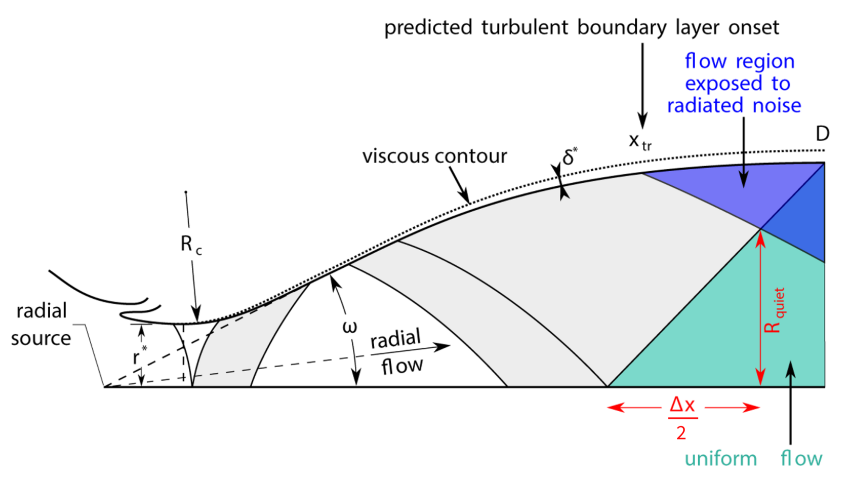


Fig 2. Overview of the design input variables needed by the pipeline, adapted from Sivells [13].

Lastly, the boundary-layer profiles are analyzed using the VESTA [12] toolkit, which applies local Linear Stability Theory (LST) to evaluate the amplification rates of key instability mechanisms in nozzle configurations, including first-mode, Görtler, Mack mode (second-mode) and, in the case of rectangular/planar nozzles, crossflow instabilities. The LST analysis is performed over a range of frequencies and spanwise wavenumbers to ensure that the most amplified disturbances are captured for each mode type.

Although LST assumes locally parallel flow and linear disturbance evolution, it remains widely used in quiet nozzle design—such as in the optimization study by Lakebrink et al. [8]—due to its low computational cost and its ability to accurately identify dominant instability trends. Its applicability in the present framework was further confirmed in [9], where comparisons with Linearized Parabolized Stability Equations (LPSE) demonstrated negligible differences in predicted growth rates, thereby validating the assumption that non-parallel and weakly non-local effects can be neglected in this context. This supports the use of LST as a fast, reliable and automatable approach for early-stage transition assessment.

Stability analysis results—such as the streamwise evolution of the N-factor, derived from the  $e^N$  method and the so-called quiet Reynolds number (computed based on the  $\Delta x$  length of the achievable quiet core, see Figure 3 where half of  $\Delta x$  is depicted)—are employed as objective metrics in the design of quiet facilities.



**Fig 3.** Visualization of half of the quiet flow region  $(\Delta x)$  used to define the quiet Reynolds number

The described methodology is directly applicable to both two-dimensional planar and axisymmetric nozzle configurations, provided the equations for the Method of Characteristics are adapted to one or the other, under either perfect gas or real gas assumptions. Its modular and automated nature ensures flexibility and adaptability to a wide range of design cases. Further details on the methodology, including the implementation of viscous corrections and validation against literature data and Navier–Stokes simulations, are provided in [9].

## 2.2. Non-Intrusive Optimization Loop

The full design pipeline, HYPNOZE  $\rightarrow$  DEKAF  $\rightarrow$  VESTA, is embedded in a *Bayesian Optimization* (BO) framework that treats the entire chain as a black-box function. This non-intrusive approach enables geometry optimization without the need for adjoint methods, manual differentiation, or solver modification. Given the relatively low dimensionality of the problem and the computational cost of each simulation (one hour per evaluation), Bayesian Optimization offers an ideal balance between accuracy and efficiency.

The optimization proceeds through the following stages, presented in Figure 4:

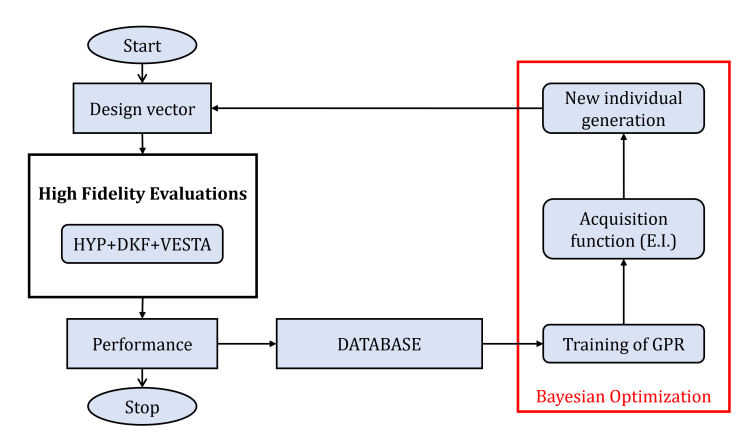


Fig 4. Bayesian Optimization process flow chart.

- 1. **Design Initialization (Start and Design Vector):** The optimization begins with an initial set of nozzle geometries, sampled using Latin Hypercube Sampling (LHS) to ensure broad coverage of the design space. Each design vector includes geometric and thermal parameters that define a candidate configuration.
- 2. **High-Fidelity Evaluation (HYP + DKF + VESTA):** Each candidate is evaluated using the full simulation pipeline. This includes hypersonic flow simulations (HYP), viscous corrections (DKF) and linear stability analysis (VESTA). The performance metrics—such as *N*-factor growth and quiet Reynolds number—are computed and stored.
- 3. **Database Update (DATABASE):** Evaluation results are added to the design database, forming the training set for surrogate modeling.
- 4. **Surrogate Model Training (Learning):** A Gaussian Process Regression (GPR) model is trained on the accumulated data. It provides predictions of performance metrics and quantifies uncertainty across the design space.
- 5. **Acquisition Function (Expected Improvement):** The Expected Improvement (EI) acquisition function guides the search by balancing *exploration* of uncertain regions and *exploitation* of promising designs. The next candidate is selected by maximizing EI.
- 6. **New Candidate Generation:** The selected design vector is passed to the simulation pipeline for evaluation, completing one optimization loop.

7. **Convergence Check (Loop and Stop):** The process iterates—updating the GPR model, reevaluating the acquisition function and generating new candidates—until an iteration number is reached.

The optimization strategy is implemented using open-source Python libraries, namely scikit-learn and scikit-optimize, ensuring transparency, reproducibility and ease of extension.

Despite relying on three independent solvers and multiple physical models, the framework remains computationally efficient. A full individual analysis and model training—encompassing geometry generation, viscous correction and local stability analysis—typically requires under one hour on a single CPU, making the methodology suitable for systematic studies and scalable to more complex configurations.

## 3. Optimization Framework

To evaluate the effectiveness of the proposed optimization methodology a two-dimensional supersonic (M=3.5) planar nozzle will be considered in the present study.

The goal is to delay the laminar-to-turbulent transition by minimizing the amplification of flow instabilities along the nozzle wall. This is achieved by optimizing geometric and thermal boundary conditions. In the following paragraphs, the objective function, reference case and optimization process results will be provided.

## 3.1. Objective Function

The N-factor method is a well-established approach for estimating transition onset in boundary-layer flows and is commonly used to guide both experimental interpretation and numerical optimization. In the context of quiet supersonic tunnels, a critical threshold of  $N_{\rm crit}=7.5$  is typically assumed, based on experimental studies such as Chen et al. [5]. This criterion provides a practical reference for assessing whether transition is likely to occur within the nozzle.

Given the freestream Mach number of (M=3.5) targeted in this study and the high quiet Reynolds ( $Re_{\Delta x}=20\times 10^6$ ), the two primary instability mechanisms considered are:

- <u>First-mode</u> instabilities, which arise from viscous–inviscid interaction in the boundary layer and typically manifest as oblique waves;
- <u>Görtler</u> instabilities, arising in concave geometries and driven by centrifugal effects induced by wall curvature.

Second-mode instabilities are not expected to be significant at this Mach number but are still included in the analysis of each individual configuration for completeness. Crossflow instabilities, on the other hand, are excluded from the current study, as their accurate prediction requires a fully three-dimensional base flow, an aspect that lies beyond the scope of the present 2D methodology and would require computationally expensive 3D simulations. Nevertheless, it should be emphasized that crossflow can play a critical role for these geometries, particularly due to the rectangular nozzle shape and the associated pressure gradients in the planar sections. Hence, the present approach may be limiting and the introduction of crossflow analyses would be essential in future investigations for planar nozzles.

Beckwith et al. [14] showed that in 2D-planar nozzles operating at Mach 3.5, Görtler instabilities tend to dominate over first-mode disturbances. Transition is commonly assessed using the composite N-factor proposed by Schneider [7], which combines the contributions of both mechanisms through an orthogonal formulation:

$$N_{\text{combined}} = \sqrt{N_{1\text{st}}^2 + N_{\text{G\"o}}^2}.$$
 (1)

This formulation is retained in the present study for the estimation of transition onset. However, because the first mode is often very weak ( $N_{\rm 1st} \ll 1$ ), the quadratic combination further suppresses its contribution, reducing sensitivity to design variations. To avoid this limitation when driving the optimization, a linear summation is introduced:

$$N_{\text{tot}} = N_{1\text{st}} + N_{\text{G\"o}},\tag{2}$$

which ensures that both instability mechanisms contribute to the metric. Accordingly, the Bayesian optimization framework minimizes

$$J = \min(N_{\mathsf{tot}}),\tag{3}$$

while transition predictions continue to be evaluated using the literature-based  $N_{combined}$ .

In addition to minimizing instability amplification, secondary design constraints are enforced to preserve geometric feasibility and flow quality, including:

- Smoothness of the nozzle contour (to avoid curvature discontinuities);
- Practical feasibility of the heating system.

## 3.2. Design Space and DoE Definition

Starting from the complete set of parameters influencing nozzle geometry (illustrated in Figure 2), the design space was reduced to a subset of key variables in order to limit computational cost while preserving performance fidelity and physical relevance.

Stagnation conditions  $(P_0, T_0)$  were fixed according to the operational constraints of VKI's internal facilities, reflecting realistic achievable operational conditions  $(P_0 = 5 \text{ bar}, T_0 = 290 \text{ K})$ . The boundary-layer start location  $(x_{BL})$  and the wall curvature radius at the throat  $(R_c)$  were also fixed to ensure consistent flow development near the throat region. Specifically,  $x_{BL}$  was placed one throat diameter upstream of the geometric throat to mimic the presence of a bleed lip, which would remove the incoming boundary layer from the contraction region. This allows a clean boundary layer to develop along the divergent section without requiring the full design of a bleed system at this stage. The wall curvature was set to  $R_c/r^* = 20$ , promoting a smooth and gradual expansion that helps suppress early curvature-driven instabilities, as recommended in previous studies [14].

The throat half-height  $r^*$  was fixed to 0.015 m to achieve a quiet Reynolds number of  $20 \times 10^6$  while maintaining nozzle compactness and manufacturability. This choice removes  $r^*$  from the list of free design variables, ensuring that the Reynolds number target is consistently met across all optimized geometries without requiring further iteration.

The remaining free design variables for the optimization are: maximum opening angle, non-dimensional length  $X_{BC}$  and the wall temperature distribution. These define the objective function as:

$$J = \min(N_{\mathsf{tot}}(\omega, X_{BC}, T(x))) \tag{4}$$

Non-dimensional length between design points B and C  $(X_{BC})$  for the transition region between the end of the radial flow region and the beginning of the uniform one is computed via Sivells' methodology [15], which prescribes favorable upper and lower bounds  $(X_{BC,\min}, X_{BC,\max})$  for the non-dimensional distance so that the Mach number at point B is ranging between 75 to 80% of the nozzle exit Mach number. To preserve flow quality and avoid expansion discontinuities,  $X_{BC}$  (illustrated in Fig. 3) is defined through a normalized design variable  $X_{BC,\%}$  ranging from 0 to 1:

$$X_{BC} = X_{BC, \min} + (X_{BC, \max} - X_{BC, \min}) \cdot X_{BC, \%}$$
 (5)

This formulation enables a smooth variation of the expansion length while staying within physically meaningful bounds.

Maximum Opening Angle  $(\omega)$  plays a critical role in the amplification of centrifugal instabilities (Görtler modes). As shown in previous studies [5], lower values of  $\omega$  promote flow stability by reducing wall curvature gradients. In this study,  $\omega$  was constrained between  $2^{\circ}$  and  $4^{\circ}$ , with the lower bound selected to prevent impractically long nozzle geometries.

Wall Temperature Distribution (T(x)) is parameterized using three intermediate control points, plus a fourth located at the nozzle exit, each defined as a percentage of the nozzle length  $(x_i/L)$ . , interpolated using spline functions. The temperature at each control point ranges from 290 K to 350 K, a range that is both practically achievable with simple heating systems and low enough to avoid deformation or

manufacturability issues. Wall temperature plays a pivotal role in boundary-layer stability, particularly near the throat region where the boundary layer is most sensitive to disturbance amplification. In this regard, targeted heating has been shown to effectively suppress first-mode growth. In particular, Demetriades [6] demonstrated that local surface heating near the throat stabilizes the laminar boundary layer by shifting the onset of transition downstream, thereby providing a passive control strategy with substantial benefits for quiet nozzle performance.

Table 1 summarizes all the design variables along with their upper and lower bounds.

**Table 1.** Design of Experiments (DoE) Parameter Matrix

	$\omega$ [deg]	<i>X<sub>BC,%</sub></i> [%]	$x_1/L$ [%]	$x_2/L$ [%]	$x_3/L$ [%]	$T_1$ [K]	$T_2$ [K]	$T_3$ [K]	$T_4$ [K]
min	2.0	0	20	45	75	290	290	290	290
max	4.0	100	40	70	95	350	350	350	350

An initial Design of Experiments (DoE) of 64 individuals was generated using Latin Hypercube Sampling (LHS) to ensure uniform coverage of the defined design space.

## 3.3. Reference Design Identification

A reference configuration was defined to represent a baseline, non-optimized nozzle design. This case assumes no active wall temperature control and uses mid-range values for all geometric parameters. It serves as a benchmark for evaluating the relative performance improvements achieved through optimization.

The reference nozzle main design parameters, are summarized in Table 2:

**Table 2.** Reference nozzle design parameters.

$M_{exit}$	$P_0$ [bar]	$T_0$ [K]	$\omega$ [deg]	$r^*$ [m]	$X_{BC,\%}$ [%]	$R_C$	$x_{BL}$	T(x)	$T_w$ [K]
3.5	5	290	3.0	0.015	0.5	20	-2 $\cdot r^*$	Constant	300

Figure 5 illustrates the geometry of the reference nozzle configuration. The plot highlights key features of interest: the ideal inviscid expansion contour generated via HYPNOZE using the Method of Characteristics (MoC, dashed line), the viscous-corrected wall shape accounting for laminar boundary-layer growth (solid line) and the downstream portion of the uniform flow region, which is expected to be under quiet flow conditions, as defined in Figure 3.

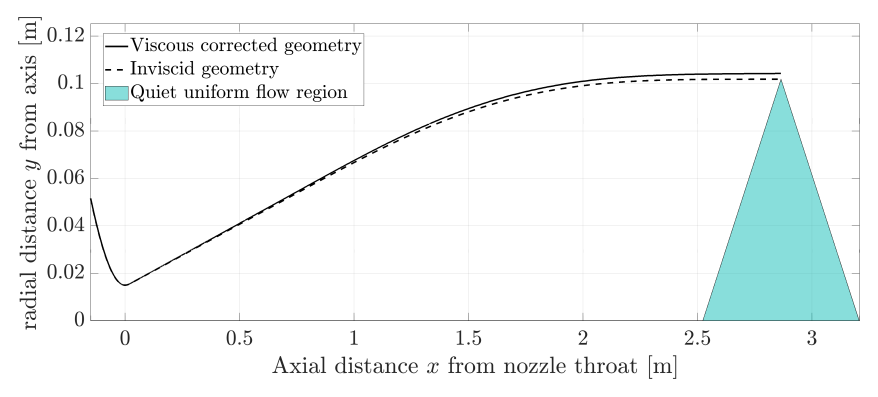
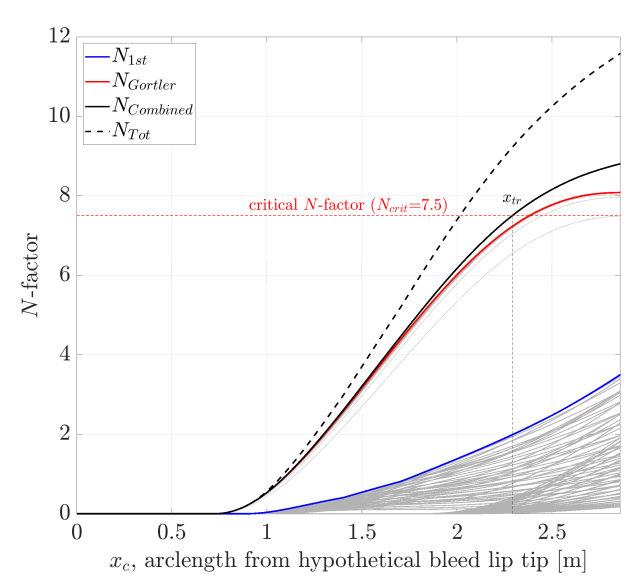


Fig 5. Reference nozzle geometry (vertically stretched for enhanced visibility).

Boundary-layer transition predictions based on Linear Stability Theory (LST) are shown in Figure 6. The first-mode instability was analyzed over a frequency range of 1 to 6 kHz, while the Görtler instability was

evaluated using a range of constant number of spanwise vortices [120-250] uniformly distributed across the nozzle width. This defines a discrete spanwise wavenumber set  $\beta = \frac{\text{width}}{N_{\text{waves}}}$ . The plot compares the amplification of each mode and their combination, clearly showing that the combined N-factor exceeds the critical threshold, thus predicting transition within the nozzle.



**Fig 6.** N-factor evolution from LST for the reference configuration. Individual mode contributions, combined and total prediction are shown ( $N_{\text{Combined}}$  from Eq. 1, used to define if transition occurs and  $N_{\text{Tot}}$  from Eq. 2, used as optimization metric term). The second-mode instability does not arise under the present flow conditions.

The corresponding transition onset location is shown in Figure 7, where the transition point—identified by a blue diamond—marks the streamwise location at which the combined N-factor exceeds the critical value. From this point onward, disturbances begin to propagate into the core flow, thereby limiting the extent of the quiet region and potentially contaminating the test section with acoustic noise.

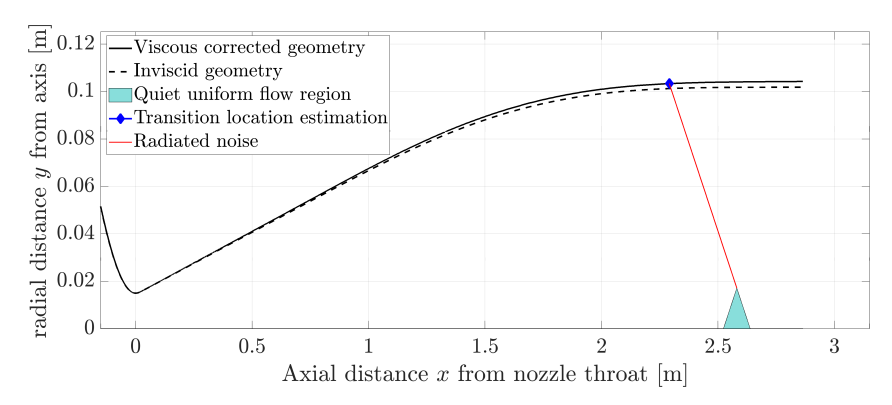


**Fig 7.** Predicted transition location based on combined N-factor. Boundary-layer thickness and transition onset are indicated.

The resulting quiet Reynolds number for the reference configuration (3.3 million) falls significantly below the desired lower bound target of 20 million, reinforcing the need for geometry optimization and active thermal control strategies to delay transition and extend the quiet flow region.

## 4. Optimization Results

A total of 150 optimization iterations were performed within the Bayesian Optimization loop. The accuracy of the surrogate model was evaluated using Leave-One-Out (LOO) cross-validation. This method tests the model's ability to predict unseen data by systematically excluding each point in turn. For the  $N_{\rm tot}$  objective, LOO yielded  $R^2=0.9755$ , meaning the surrogate model captures over 97% of the variance in the true model. This strong predictive performance is illustrated in Figure 8, where points closely follow the diagonal, indicating very good agreement between predicted and actual values.

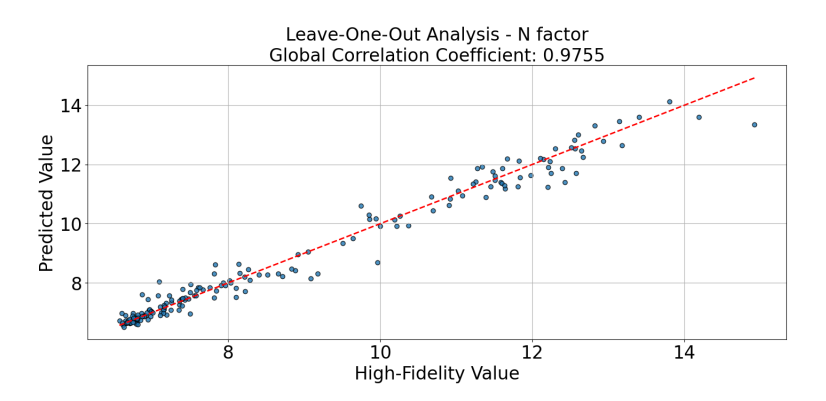


Fig 8. Leave-One-Out analysis for the surrogate model built for supersonic quiet nozzle design

Figure 9 presents the complete set of simulations via a parallel coordinate plot, combining the initial DoE and all subsequent optimization samples. In Figure 10, only the best-performing configurations—those with the lowest N-factor—are highlighted to illustrate the clustering behavior of optimal designs.

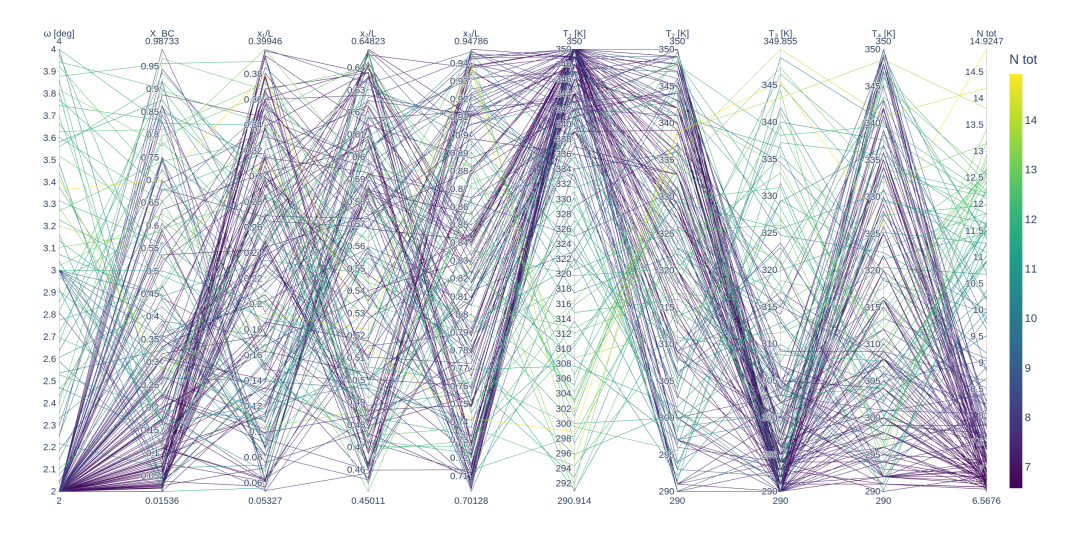
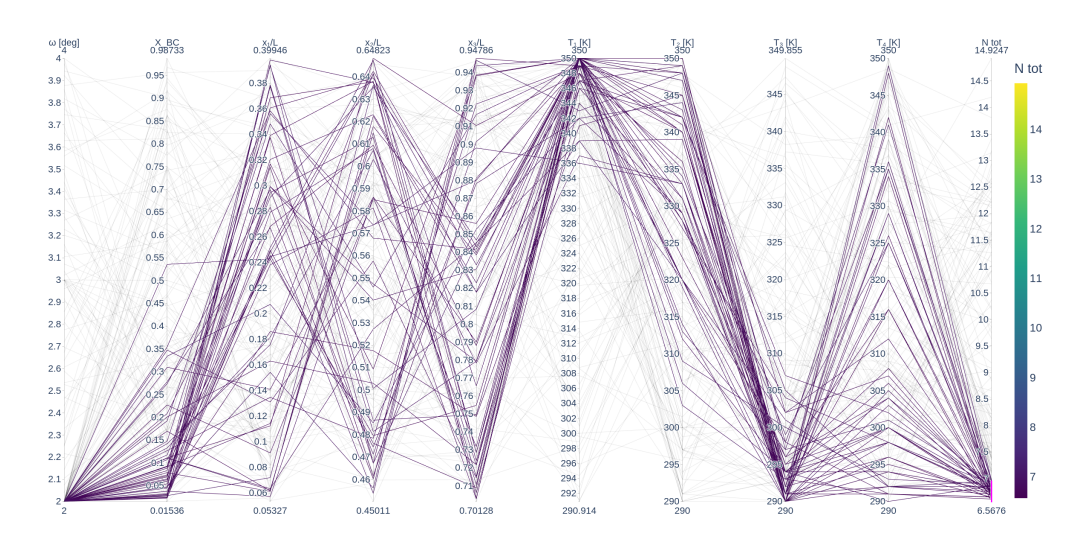


Fig 9. Dynamic parallel coordinate plot showing the optimization trajectories.

These clustered patterns suggest that specific geometric trends consistently lead to lower instability levels. To better understand the physical mechanisms behind these optimal solutions, each key geometric parameter is examined individually below.

- Throat Opening Angle ( $\omega$ ): Optimal solutions consistently lie at the lower end of the allowed range ( $\approx 2^{\circ}$ ), confirming the stabilizing role of shallow expansions. Low  $\omega$  tackles Görtler-type instabilities by minimizing the length of the concave region and thus centrifugal effects.
- Non-dimensional Length ( $X_{BC}$ ): High-performing configurations exhibit low  $X_{BC}$  values, corresponding to a shorter extent of the concave flow region. This reduction appears to limit the



**Fig 10.** Dynamic parallel coordinate plot showing the optimization trajectories and highlighting best-performing configurations based on minimum N-factor.

development of concave-flow instabilities. The clustering near the lower bound suggests a saturation trend, motivating future exploration beyond the current limits.

• Wall Temperature Control (T(x)): The wall temperature distribution is parameterized by control points:  $x_1$ ,  $x_2$  and  $x_3$  define the spatial locations, while  $T_1$  through  $T_4$  define the imposed temperatures at those points and at the nozzle exit.

# Key insights include:

- Location of control points  $(x_1/L, x_2/L, x_3/L)$ : No dominant trend emerged; the ranges were pre-constrained within defined nozzle zones, making the temperature values more impactful than their exact locations.
- High temperatures near the throat  $(T_1, T_2)$ : Elevated values in the throat region correlate with improved performance. This stabilizes early-stage first-mode waves, consistent with prior studies [7].
- Strong cooling at  $T_3$ : All top-performing designs feature a steep drop at  $T_3$ , indicating a critical region where cooling mitigates the amplification of first-mode instabilities. This behavior aligns with the need to decrease the mean temperature near the maximum growth zone of first-mode waves, shifting them toward more stable regimes.
- No clear trend for  $T_4$  (exit temperature): The terminal wall temperature appears to have minimal influence on the transition process, though this may warrant further study and will be addressed in Section 4.1.

To further support these findings, a global sensitivity analysis based on Sobol's indices [16] was conducted on the trained surrogate model. Figure 11 displays both the first-order  $(S_1)$  and total-order  $(S_T)$  indices. The results confirm the dominant influence of  $T_1$ ,  $T_3$  and  $\omega$ , in agreement with the physical mechanisms outlined above. Notably, the difference between  $S_1$  and  $S_T$  for  $S_2$  and  $S_3$  indicates the presence of strong parameter interactions.

To complement the Sobol sensitivity analysis, Self-Organizing Maps (SOMs) [17] were employed as an unsupervised clustering technique to visualize high-dimensional patterns in the optimized dataset (see Figure 12). The SOM projects the parameter space onto a two-dimensional lattice, highlighting parameter interdependence and convergence pathways across the BO iterations.

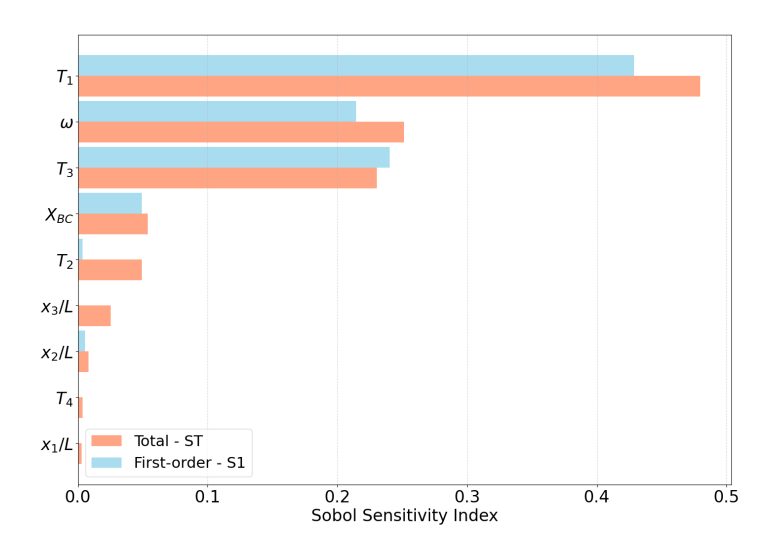
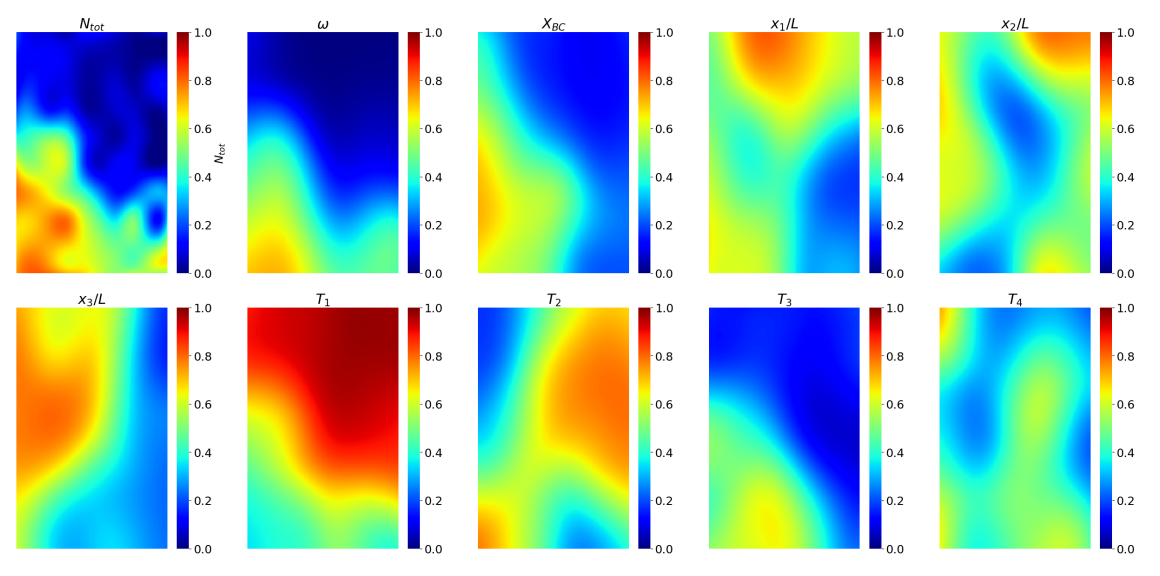


Fig 11. Sensitivity analysis of design parameters using variance based Sobol methodology.

The SOM visualization confirms trends already observed in the parallel coordinate plots and Sobol analysis:

- Regions of high performance are clearly localized and clustered on the SOM map for low  $\omega$  and sharp temperature drops from high  $T_1$  to low  $T_3$ .
- The highest-performing individuals tend to occupy contiguous regions associated with low  $\omega$ , high  $T_1$  and sharp drops in  $T_3$ .
- Parameters like  $x_1$ – $x_3$  and  $T_4$  exhibit more uniform distribution across the map, further supporting their lower sensitivity.



**Fig 12.** Self-Organizing-Maps, all values are nondimensionalized within their operational defined bounds.

Together, the combined use of GPR modeling, BO-driven sampling, Sobol analysis and SOM visualization

offers a multi-perspective view of the optimization landscape, enabling both quantitative sensitivity assessment and intuitive pattern recognition across high-dimensional parameter spaces.

An important observation is that the best individuals (i.e., with lowest  $N_{\text{Tot}}$ -factor envelope) do not exhibit transition within the nozzle, hence  $N_{\text{Combined} < 7.5}$ , implying that the selected parameter combinations succeed in maintaining laminar flow throughout the contour. These configurations should therefore be favored in quiet wind tunnel applications.

# 4.1. Analysis of Competing Optimal Designs:

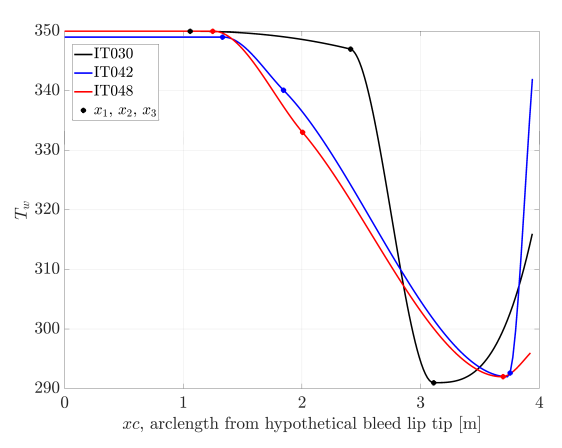
While the optimization achieved convergence within a narrow performance band of the objective function, the resulting high-performing candidates reveal non-negligible variation in their parameter combinations, especially in the wall temperature distributions. This suggests the existence of multiple viable stability control strategies within the design space. To further understand the physical mechanisms underpinning these solutions, we now analyze three representative optimal designs in detail. Despite yielding comparable N-factor values, these candidates differ in thermal layout, offering valuable insights into the trade-offs and robustness of instability suppression strategies.

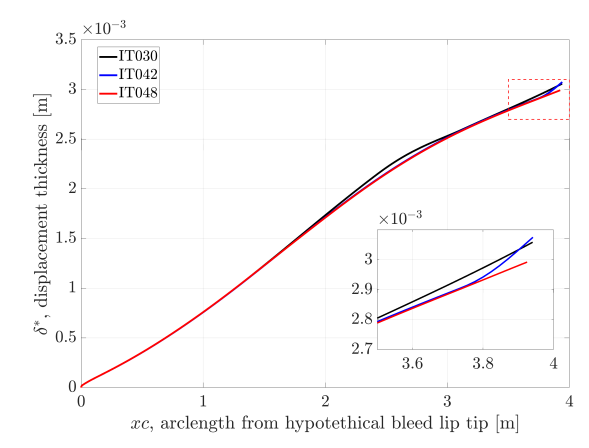
Table 3 summarizes the individuals characteristics:

IT#  $X_{BC,\%}$  [%]  $x_1/L$  [%]  $x_2/L$  [%]  $x_3/L$  [%]  $\omega$  [deg]  $T_1$  [K]  $T_2$  [K]  $T_3$  [K]  $T_4$  [K]  $N_{tot}$ IT030 2.0 7 27 60 80 350 347 292 316 6.58 IT042 2.0 7 33 47 94 348 340 292 342 6.61 2.0 3 32 51 94 350 292 296 IT048 333 6.62

**Table 3.** Optimal candidates design parameters.

As defined in Section 3.1, one of the constraints imposed during optimization was smoothness of the wall contour and feasibility of thermal implementation. Upon examining both the wall temperature profile and the viscous displacement thickness evolution, displayed in Figure 13, configuration IT042 was excluded due to its nonphysical characteristics. In particular, the design exhibits a steep thermal rise near the end of the nozzle, which would be difficult to reproduce under practical conditions. Additionally, the corresponding spike in the  $\delta^*$  profile introduces a curvature inflection in the nozzle contour that could result in surface discontinuities and non-uniform flow behavior.





(a) Wall temperature distributions

(b) Boundary layer displacement thickness

Fig 13. Comparison between optimal designs.

The remaining two configurations, IT030 and IT048, satisfy all geometric and physical constraints and are further analyzed in Figure 14. This figure compares their N-factor evolution and local modal growth rates. Both candidates exhibit subcritical N-factor values (below 7.5) at the nozzle exit, indicating no

transition is expected under linear stability assumptions. However, to further assess which design offers better robustness, attention is shifted from integrated N-factors to the local growth rates  $\alpha_i$ , particularly in the context of mode interaction.

Since Görtler instability is primarily geometry-driven and both designs share similar expansion characteristics (e.g., identical or nearly identical  $X_{BC}$ ), the peak of Görtler amplification occurs at comparable streamwise locations. In contrast, first-mode instability is highly sensitive to thermal gradients and the different temperature distributions lead to distinct patterns of modal growth. Notably, while IT030 exhibits slightly lower combined N-factors, IT048 demonstrates significantly lower first-mode growth near the Görtler peak. This separation in peak amplification reduces the likelihood of nonlinear interactions between the two instability mechanisms.

To quantify this effect, a new metric was introduced: the infinity norm of the summed growth rates, defined as

$$\alpha_{i,\mathrm{Tot}} = \alpha_{i,\mathrm{1st}} + \alpha_{i,\mathrm{G\"o}}$$

This metric captures the worst-case concurrent amplification and highlights IT048 as the most robust candidate when considering overall instability evolution, not just the final integrated amplification at the nozzle exit.

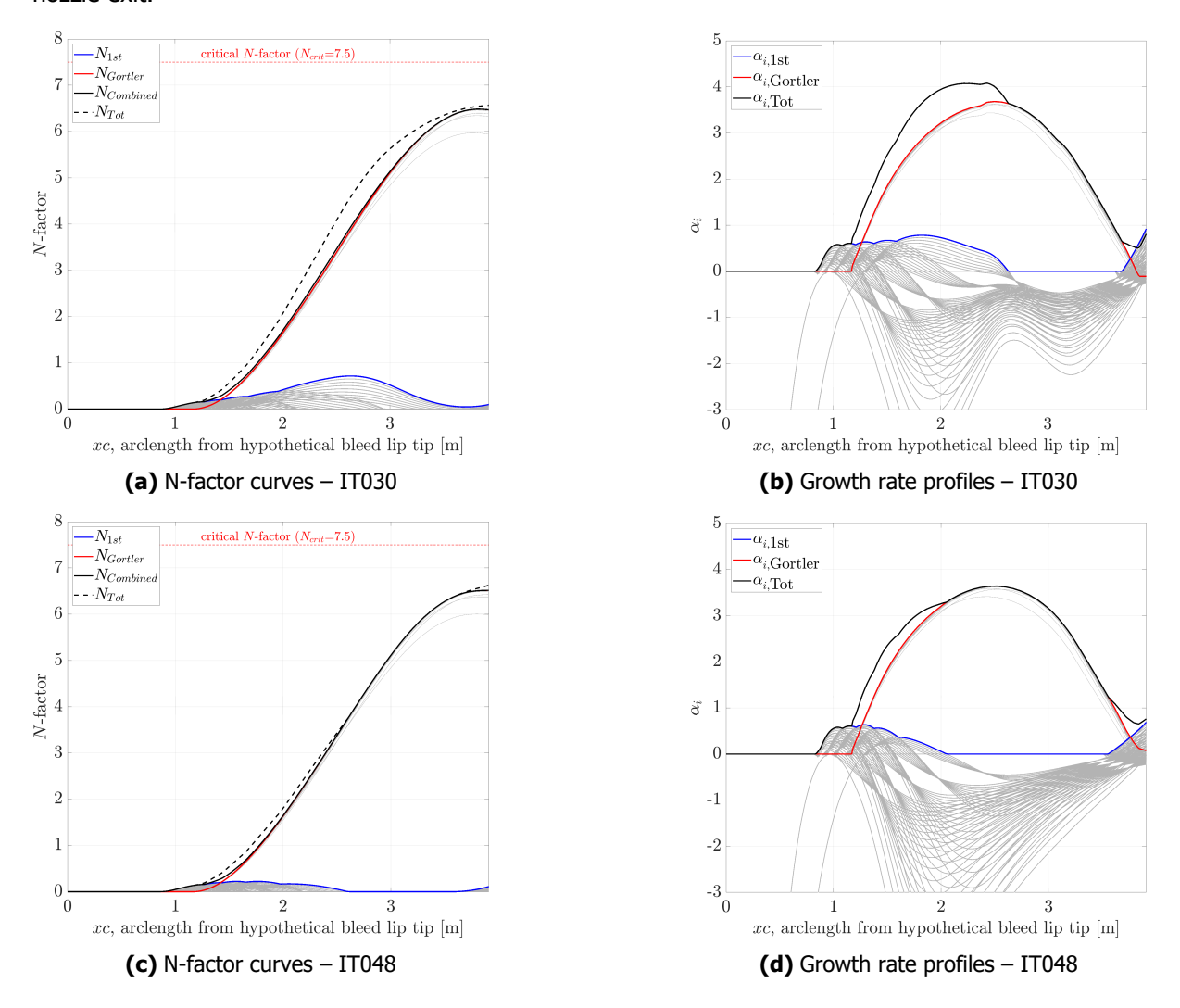


**Fig 14.** Comparison of N-factor evolution and modal growth rates for IT030 and IT048 configurations.

## 5. Conclusion

This study presents a robust and flexible optimization framework for the design of quiet supersonic and hypersonic wind tunnels. The proposed approach leverages Bayesian optimization to efficiently explore complex design spaces and identify low-noise configurations with minimal computational cost. Despite using a limited number of high-fidelity evaluations, the surrogate model rapidly achieved high predictive accuracy and consistently guided the search toward optimal solutions.

The framework is fully modular and can be extended to different Mach number regimes, including hypersonic applications, by incorporating additional instability mechanisms such as second-mode. Its structure allows easy adaptation through the inclusion of new design variables and stability metrics tailored to specific operating conditions or flow physics.

Even though crossflow effects were not included in the present 2D formulation, the results yield valuable insights into instability suppression along the diverging nozzle walls. In particular, the analysis highlighted the stabilizing influence of low transition length ( $X_{\rm BC}$ ) values and the importance of maximizing wall temperatures in targeted regions. Furthermore, a new instability metric—based on the minimum combined growth rate—was introduced to discriminate among similarly performing candidates, offering a more nuanced assessment of robustness against nonlinear interactions.

Overall, the proposed methodology demonstrates strong potential for application in the early design stages of quiet tunnel geometries, enabling rapid iteration and deeper understanding of critical flow-stabilizing mechanisms.

## **Acknowledgments**

This work was carried out under ESA contract No. 4000139380. The authors gratefully acknowledge Dr. M. Capriati and V. Romano for their valuable discussions regarding the interpretation of results and the implementation of the optimization framework.

## References

- [1] O. Chazot, A. Gülhan, K. Hannemann, M. McGilvray, L. Serre, P. Tran and J. Steelant. Need for low-noise high-speed facilities in Europe. *International Conference on Flight vehicles, Aerother-modynamics and Re-entry Missions and Engineering (FAR)*, 2019.
- [2] S. P. Schneider. Effects of high-speed tunnel noise on laminar-turbulent transition. *Journal of Spacecraft and Rockets*, 38(3), 2001.
- [3] J. Laufer. Aerodynamic noise in supersonic wind tunnels. *Journal of Aeronautical Sciences*, 28(9):685-692, September, 1961.
- [4] I. E. Beckwith and B. B. Holley. Görtler vortices and transition in wall boundary layers of two Mach 5 nozzles. (TP-1869), August 1981.
- [5] F.-J. Chen, M. R. Malik and I. E. Beckwith. Instabilities and transition in the wall boundary layers of low-disturbance supersonic nozzles. (AIAA-85-1573), July 1985.
- [6] A. Demetriades. Stabilization of a nozzle boundary layer by local surface heating. *AIAA Journal*, 34(12):2490–2495, 1996.
- [7] S. P. Schneider. Design of a Mach-6 quiet-flow wind-tunnel using the eN method for transition estimation. *In 36th AIAA Aerospace Sciences Meeting Exhibit, number AIAA paper 1998-0547, January,* 1998.
- [8] M. T. Lakebrink, K. G. Bowcutt, T. Winfree and C. C. Huffman. Optimization of a Mach-6 quiet wind-tunnel nozzle. *Journal of Spacecraft and Rockets*, 55(2):315-321, March 2018.
- [9] A. Testa, P. Schrooyen, G. Grossir and J. Steelant. Advanced design methodology for laminar boundary layer control in axisymmetric nozzles. *11th European Conference for AeroSpace Sciences (EUCASS)*, 2025.

- [10] G. Grossir and O. Chazot. Design of axisymmetric contoured nozzles for calorically and thermally imperfect gases using the Hypnoze code. *In HiSST: 2nd International Conference on High-Speed Vehicle Science Technology, HiSST-2022-0038.*, 2022.
- [11] F. Miró Miró, K. Groot, E.S. Beyak, A.J. Moyes, F. Pinna and H.L. Reed. DEKAF: an open-source spectral boundary-layer solver. *Tech. Rep. VKI-TM-56, von Karman Institute for Fluid Dynamics Texas A&M University Delft University of Technology.*
- [12] F. Pinna. *Numerical study of stability of flows from low to high Mach number.* PhD thesis, von Karman Institute for Fluid Dynamics Universitá di Roma "La Sapienza", 2012.
- [13] J. C. Sivells. Aerodynamic design of axisymmetric hypersonic wind tunnel nozzles. *Journal of Spacecraft and Rockets*, 7(11):1292–1299, 1970.
- [14] I. Beckwith, F.-J. Chen and M. R. Malik. Design and fabrication requirements for low noise supersonic hypersonic wind tunnels. *In Research in Natural Laminar Flow and Laminar-Flow Control, December 1987.*
- [15] J. C. Sivells. A computer program for the aerodynamic design of axisymmetric and planar nozzles for supersonic and hypersonic wind tunnels. Technical Report ADA062944, Arnold Engineering Development Center, Arnold AFB, TN, December 1978. Final report, Dec. 1975 Oct. 1977.
- [16] I. M. Sobol. Global sensitivity indices for nonlinear mathematical models and their Monte Carlo estimates. *Mathematics and Computers in Simulation*, 55(1-3):271–280, 2001.
- [17] T. Kohonen. Self-organized formation of topologically correct feature maps. *Biological Cybernetics*, 43(1):59–69, 1982.